Influence of biomass burning from South Asia at a high-altitude mountain receptor site in China

Jing Zheng[1], Min Hu[1,*], Zhuofei Du[1], Dongjie Shang[1], Zhaoheng Gong[2,a], Yanhong Qin[1], Jingyao Fang[1], Fangting Gu[1], Mengren Li[1], Jianfei Peng[1], Jie Li[3], Yuqia Zhang[3], Xiaofeng Huang[2], Lingyan He[2], Yusheng Wu[1], Song Guo[1]

[1]State Key Joint Laboratory of Environmental Simulation and Pollution Control, College of Environmental Sciences and Engineering, Peking University, Beijing, China

[2]Key Laboratory for Urban Habitat Environmental Science and Technology, School of Environment and Energy, Peking University Shenzhen Graduate School, Shenzhen, China

[3]State Key Laboratory of Atmospheric Boundary Layer Physics and Atmospheric Chemistry (LAPC), Nansen-Zhu International Research Center (NZC), Institute of Atmospheric Physics, Chinese Academy of Sciences, Beijing, China

* *Correspondence to*: minhu@pku.edu.cn

[a] Now at John A. Paulson School of Engineering and Applied Sciences, Harvard University, Cambridge, Massachusetts, 02138, United States

Abstract

Highly time-resolved in-situ measurements of airborne particles were made at Mt. Yulong (3410 m above sea level) on the southeastern edge of the Tibetan Plateau in China from 22nd March to 14th April in 2015. Detailed chemical composition was measured by a high-resolution time-of-flight aerosol mass spectrometer together with other online instruments. Average mass concentration of the submicron particles (PM_1) was 5.7 ± 5.4 μg m^{-3} during the field campaign, ranging from 0.1 μg m^{-3} up to 33.3 μg m^{-3}. Organic aerosol (OA) was the dominant component in PM_1, with a fraction of 68 %. Three OA factors, i.e., biomass-burning organic aerosol (BBOA), biomass-burning-influenced oxygenated organic aerosol (OOA-BB) and oxygenated organic aerosol (OOA), were resolved using positive matrix factorization analysis. The two oxygenated OA factors accounted for 87 % of the total OA mass. Three biomass burning events were identified by examining the enhancement of black carbon concentrations and the f_{60} (the ratio of the signal at m/z 60 from the mass spectrum to the total signal of OA).

Back trajectories of air masses and satellite fire map data were integrated to identify the biomass burning locations and pollutants transport. The western air masses from South Asia with active biomass burning activities transported large amount of air pollutants, resulting in elevated organic concentrations up to 4-fold higher than that of the background condition. This study at Mt. Yulong characterizes the tropospheric background aerosols of the Tibetan Plateau during pre-monsoon season, and provides clear evidence that the southeastern edge of the Tibetan Plateau was affected by transport of anthropogenic aerosols from South Asia.

1 Introduction

Aerosols play an important role in the radiative balance in earth's atmosphere, with their radiative forcing still having large uncertainties (IPCC, 2013). Biomass burning emission is one of the dominant sources of atmospheric particles (von Schneidemesser et al., 2015), contributing up to 90 % of the primary organic aerosol in the global scale (Bond et al., 2004) and more than half of the total organic aerosol mass in areas with significant biomass burning influences (e.g. Yangtze River Delta region in China, and Indian Peninsula) (Zhang et al., 2015;Engling and Gelencser, 2010). Given the long atmospheric lifetime of aerosols, even remote areas can sometimes be influenced by the transportation of air pollutants from areas with active biomass burnings (Bougiatioti et al., 2014). In terms of the deterioration of air quality and climate change in those remote areas, great scientific interest has arisen focusing on the impacts on biomass burning (Lau et al., 2010;Qian et al., 2011).

The Tibetan Plateau is the largest and highest plateau in the world, and is often regarded as the "Third Pole". It is surrounded by a ring of high-elevated mountain ranges, which were considered as blocks for transportations of air pollutants from its vicinity (Wang and French, 1994). Since this vast land has a relatively low population density with minor anthropogenic influences, the Tibetan Plateau has been considered as a natural background of the Eurasian continent (Ming et al., 2010;Wan et al., 2015). In recent years, studies have presented convincing evidence for the transport route of air pollutants climbing over the Himalayas, especially during pre-monsoon season, coinciding with the annual intensive fire season in South and Southeast Asia (Streets et al., 2003;Marinoni et al., 2010;Cong et al., 2015b). A westerly dry circulation helps to build up the smoke plume against the Himalayan ridges, elevating to 3-5 km in altitude (Bonasoni et al., 2010;Xia et al., 2011). Subsequently, downward glacier wind of local mountain breeze circulation brings biomass burning related air pollutants down to the mountain valley (Cong et al., 2015b;Lüthi et al., 2015).

A host of studies based on field campaigns have amassed an impressive amount of information describing the biomass burning influence on different areas of the Tibetan Plateau (Decesari et al., 2010;Zhao et al., 2013;Xu et al., 2015). Those studies were mostly approached by analyzing the temporal and spatial variations of atmospheric composition based on filter measurements. The strong correlation of carbonaceous aerosol with biomass burning tracers K^+ and levoglucosan pointed out the origins of aerosols (Cong et al., 2015a). Biomass burning organic aerosol (BBOA) was also found to be a major fraction of organic aerosol (OA), with a 15 % contribution to the total OA mass (Du et al., 2015). Xu et al. (2013) and You et al. (2016) also presented convincing evidence about biomass burning impacts by analyzing chemical components in glaciers collected in the Tibetan Plateau. Most of previous studies were based on offline analysis using filter or glacier samples, which were limited to low time resolution, making it difficult to follow the aging process of biomass burning aerosol. Thus in-situ measurements of aerosol chemical characterization with high time resolution are needed, so as to have a deep understanding of the sources and evolution of the particulate matter.

In this study, the influence of biomass burning from South Asia on the Tibetan Plateau has been analyzed. The results can serve as inputs or constraints for global climate model simulations. By examining the aerosol properties as a function of chemical composition at Mt. Yulong at the southeastern edge of the Tibetan Plateau, this study sheds light on the evolution processes of OA. Positive matrix factorization analysis has been conducted to resolve different sources of OA. And the influence of biomass burning from South Asia transported over long distances to the Tibetan Plateau background environment during pre-monsoon season has been characterized.

2 Method

2.1 Site description and meteorological conditions during the campaign

In this study, we conducted an intensive observation at the site on Mt. Yulong (27.2 °N, 100.2 °E), with an altitude of 3410 m a.s.l., northwestern Yunnan Province, China (Fig. 1). Since Mt. Yulong is lying in the transition zone extending from the low altitudes of the Yunnan Plateau (~ 3000 a.s.l.) to the high altitude of the Tibetan Plateau (~ 5000 a.s.l.), it is on the transport route of pollutants from South Asia to inland China, making it an ideal site to observe the influence of regional and long-range transport of polluted air masses. This station is a member of the National Atmospheric Watch Network coordinated by the Chinese Environmental Monitoring Center. The famous tourist attraction Lijiang Old Town locates more than 20 km away and 1000 m lower than the elevation of the station. The observation period was conducted during the pre-monsoon season of the Tibetan Plateau, from 22nd March to 14th April 2015, corresponding to the annual biomass burning seasons in South Asia. Since the season was cold with sparse visitors in Lijiang old city, the influence of local emissions from residents and visitors remained low compared with other seasons.

2.2 Measurements and data processing

A high resolution time-of-flight aerosol mass spectrometer (AMS, Aerodyne Research Inc.) was deployed to measure the highly time-resolved chemical composition of sub-micron, non-refractory aerosols (Table S1). The standard operation procedures of the AMS has been described in detail in Canagaratna et al. (2007). The time resolution was 5 min for AMS measurement, with 2.5 min in V mode to obtain mass concentration, and 2.5 min in W mode for HR mass spectrum of organics. The detection limits (DL) of organic, sulfate, nitrate, ammonium and chloride were 0.07, 0.004, 0.003, 0.005 and 0.01 $\mu g\ m^{-3}$, respectively. During most time of the campaign, the mass concentrations of chloride were below its DL, and including it would lower the total signal to noise ratio, therefore it is omitted from the analysis.

The AMS data was analyzed using the standard AMS data analysis software, i.e., SQUIRREL (version 1.57) for unit resolution mass spectrum data, and PIKA (version 1.16) for high resolution mass spectra data. Calibrations of the AMS on flow rate and ionization efficiency were conducted each week. To account for the particle loss due to the bounce of particles on the vaporizer, collection efficiencies were calculated and applied for data correction based on the method described by Middlebrook et al. (2012). In this study, the collection efficiencies varied from 0.5 to 0.9.

The high resolution organic aerosol spectra were further apportioned to different sources by positive matrix factorization (PMF) analysis (Paatero and Tapper, 1994;Ulbrich et al., 2009). The solution was validated by the characteristics of resolved mass spectra, as well as the comparison of temporal variations between each factor and external species (e.g. acetonitrile).

Other online instruments were also deployed at the site (Table S1). A scanning mobility particle sizer (SMPS, TSI Inc.) was used to measure particle number size distribution for particle mobility diameters ranging from 15 to 760 nm, with a time resolution of 5 min. An Aethalometer (Magee Scientific) was deployed to measure the aerosol light absorption coefficients σ_{ap} at its seven wavelengths, ranging from 370 to 950 nm. Black carbon (BC) concentration is determined by σ_{ap} at 880 nm using the default mass attenuation cross sections of 16.6 m^2 g^{-1} (Fröhlich et al., 2015). Acetonitrile was measured by a gas chromatographer with mass spectrometer and flame ionization detectors (GC–MS/FID) with a time resolution of 1 hour. Technical details of this self-made instrument were described elsewhere (Wang et al., 2016).

Meteorological parameters, including relative humidity, temperature, wind direction and wind speed, were continuously monitored on the site during the campaign. The low temperature (5 ℃ for the whole campaign average) and heavy snow eliminated the influence of biogenic emissions to this site during the campaign.

2.3 Back trajectory analysis and fire maps

To explore the influence of regional biomass burning activities on aerosol properties during the campaign, the Weather Research and Forecasting (WRF) model (version 3.61, www.wrf-model.org/index.php) was used to investigate the meteorological conditions and to compute trajectories of air masses arriving at Mt. Yulong. The original data for WRF model are available from National Centers for Environmental Prediction (NCEP) Final (FNL) Operational Global Analysis data (http://rda.ucar.edu). 48-h back trajectories were calculated every 6 hours from March 22nd to April 14th, using a starting height at 600 m above the ground level of the site.

Active fire points were obtained from the Fire Information for Resource Management System (FIRMS), which is provided by the Moderate Resolution Imaging Spectroradiometer (MODIS) satellite (https://firms.modaps.eosdis.nasa.gov/firemap/, last accessed on Aug. 26, 2016).

3 Results

3.1 Concentrations and chemical compositions of submicron aerosols

The time series of submicron aerosol compositions as well as meteorological conditions are shown in Fig. 2. The average PM_1 concentration was 5.7 ± 5.4 μg m^{-3}, with a range of 0.1 μg m^{-3} – 33.3 μg m^{-3}. This result was similar to previous observations at the Northern Tibetan Plateau, where Du et al. (2015) reported an average PM_1 concentration of 11.4 μg m^{-3} in the autumn of 2013, and Xu et al. (2014a) reported an annual average $PM_{2.5}$ concentration of 9.5 μg m^{-3} from 2006 to 2007. The averaged PM_1 concentration was much lower than those measured at urban and downwind sites of China (e.g., Huang et al., 2013;Xu et al., 2014b), but was three times higher than the 1.7 μg m^{-3} at a background site in Europe in March 2004 (Sjogren et al., 2008), and ten times higher than that measured at the same background site in the spring of 2013 (Fröhlich et al., 2015). These huge differences indicate that anthropogenic pollutions in South Asia may have resulted in the elevation of aerosol concentrations to levels above the natural background level.

Averaged aerosol composition of PM_1 is shown in the pie chart (Fig. 3(a)). The PM_1 chemical composition was dominated by organic components, which accounted for 68 %, followed by sulfate (14 %). The minor contribution of nitrate to PM_1 (4 %) can be explained by the lack of nearby anthropogenic sources for precursors (e.g., HONO, N_2O_5) (Du et al., 2015). This result presents a similar picture as those observed at remote sites in the northern hemisphere (Zhang et al., 2011), as well as at a high altitude site in Europe (Ripoll et al., 2015). Compared with urban or regional areas in China, where secondary inorganic species including sulfate, nitrate and ammonium typically contribute to over one half of the total mass concentrations, the result at this site is quite unique (Huang et al., 2010;Huang et al., 2012;Xu et al., 2014b).

Figure 3(b) shows the relative contribution of major chemical components as a function of PM_1 mass concentrations, as well as the probability density of PM_1 mass loading. PM_1 concentrations below 5 μg m^{-3} showed the highest probability (68 %). The fractions of organics and BC increase slightly with the increasing of PM_1 concentrations, showing that they were the main contributors to the pollution episodes in Mt. Yulong.

The PM_1 components did not show distinct diel variations, but remained relatively constant during the whole day, as shown in Fig. 3(c). This is similar to the findings at the Puy-de-Dôme station in central France, and the Montsec station in western Mediterranean Basin (Freney et al., 2011;Ripoll et al., 2015). Strong long-range transport of air masses with few local emissions could blur the diel cycles, since the air-mass transportations occurred regardless of the local time of the day.

3.2 Characterization of organic aerosol

3.2.1 Elemental compositions of organic aerosol

The elemental composition was calculated from high resolution mass spectra of organics obtained by AMS, using the method developed by Canagaratna et al. (2015). Compared with the previous method (Aiken et al., 2007;2008), the ratio of O/C and H/C are typically increased by 20 % and 7 %, respectively. Bulk OA was mainly composed of carbon and oxygen, with minor contributions from hydrogen and nitrogen, and had an average molecular formula of $C_1H_{1.4}O_{1.1}N_{0.04}$. The fragments of organics were grouped into five types according to the existence of C, H, O or N atoms. $C_xH_y^+$ were only 21 % of the total organic signal, while the oxygenated fraction ($C_xH_yO_z^+$) accounted for 68 % of the total OA, which is higher than those measured at urban and downwind site (30-41 %) (Huang et al., 2011;Sun et al., 2011;Hu et al., 2013). The average OM/OC and O/C ratios for the whole campaign were 2.63 and 1.11, respectively, and were similar to those measured in the north eastern region of the Tibetan Plateau (OM/OC 2.75, O/C 1.16) (Xu et al., 2015). These results are slightly higher than the elemental ratios measured at another remote site (OM/OC: 2.4, O/C: 0.9) in the eastern Mediterranean (Bougiatioti et al., 2014), probably due to the mixture of free troposphere aerosol after a long time of processing before arriving at this high altitude site. The extremely high value of OM/OC reflects the highly oxidized nature of OA in the Tibetan Plateau.

3.2.2 Source apportionment of organic aerosol

PMF analysis was performed to investigate the sources of OA measured at Mt. Yulong. Three factors were resolved, including a biomass burning organic aerosol (BBOA), an oxygenated biomass-burning-influenced organic aerosol (OOA-BB), and an oxygenated organic aerosol (OOA). Details of the PMF analysis can be found in the supplement. The mass spectra of the three factors are shown in Fig. 4. The time series of the three factors and an external species (acetonitrile) are plotted in Fig. 5.

3.2.2.1 BBOA

BBOA has been frequently identified in previous studies at urban and regional sites (Zhang et al., 2011). The mass spectrum of BBOA has a notable contribution from m/z 60 (mainly $C_2H_4O_2^+$, contributing 3.1 % of the total mass spectra), which is from fragmentation of levoglucason. As shown in Table 1, the mass spectrum correlates well with the samples from an aircraft measurement above a large forest fire (Brito et al., 2014), and well with the samples from biomass burning simulation system in the laboratory (He et al., 2010). BBOA has an O/C ratio of 0.37, presenting a similar level to previous studies (Aiken et al., 2008;He et al., 2010). The time series of BBOA correlates very well with K^+ based on filter analysis (Pearson R=0.92, N=13). The factor was also confirmed to be BBOA, since it has a similar temporal variation to that of acetonitrile (Fig. 5), a gas phase tracer for biomass burning.

The average concentration of BBOA was 0.5 μg m^{-3} for the whole campaign, accounting for 13 % of the total OA mass, with a maximum contribution at 61 % (Fig. 6 (a)). The spikes in the time series of BBOA indicate that a fraction of BBOA was contributed by primary sources nearby, possibly occasional biomass burning activities for domestic heating and cooking. The increasing fraction of BBOA as a function of total OA concentrations points to contributions from biomass burning activities during the pollution episodes (Fig. 6 (b)).

3.2.2.2 OOA-BB

The mass spectrum of OOA-BB factor was dominated by $C_xH_yO_z^+$ fragments, especially org29 (CHO^+), org43 ($C_2H_3O^+$) and org44 (CO_2^+). The spectrum of OOA-BB in this study well correlated with aged BBOA obtained 3 hours downwind of a forest fire (Brito et al., 2014) (Pearson R=0.97, N=100). It is qualitatively similar to published OOA-BB spectra from aged BB plumes in China during the harvest seasons (Zhang et al., 2015), and also presented many similarities to those of OOA2-BBOA resolved in the metropolitan area of Paris (Crippa et al., 2013).

The average concentration of OOA-BB was 0.9 μg m^{-3} for the whole campaign, accounting for 22 % of the total OA mass. Compared with BBOA measured near sources, OOA-BB shows a higher oxygenated degree, with an O/C of 0.85, and a lower fraction of m/z 60 (0.6 %), as a result of the oxidation of primary levoglucosan-type species (Jolleys et al., 2015). This oxidation process can be quick in elevating the oxidation state and reducing f_{60} (calculated as the ratio of the signal at m/z 60 to the total OA signal), which is also reported in another study by Minguillón et al. (2015). As the plumes originated from South Asia were measured at a distance of several hundred kilometers downwind, emissions would have undergone substantial aging prior to sampling. The aging process includes both the gas-phase oxidation of semi volatile species from biomass burning sources and heterogeneous or homogeneous reactions of existing particles during long-range transport (Bougiatioti et al., 2014). The time series of OOA-BB and BBOA yield modest correlations with BC (Pearson R=0.62 and 0.65, N=5940). If we focus on the total biomass burning related organic aerosols (OOA-BB + BBOA), the R value for its correlation with BC would increase to 0.76 (N=5940), indicating biomass burning related OA originated from the same source as BC.

3.2.2.3 OOA

OOA is described as highly oxidized, aged particles formed after long-range transportation and processing. The mass spectral properties of OOA are defined by having a dominant peak at m/z 44 (mainly CO_2^+) and other ions of $C_xH_yO_z^+$. The highly oxidized nature of OOA is also reflected by its high O/C ratio of 1.45. The mass spectrum of OOA resembles that of more oxidized OOA (MO-OOA) in Beijing well (Pearson R=0.69, N=100) (Hu et al., 2016).

OOA has an average concentration of 2.6 μg m^{-3}, accounting for 65 % of the total OA mass. Unlike previous studies at urban or regional sites (Jimenez et al., 2009;Li et al., 2015;Hu et al., 2016), the time series of OOA did not agree well with that of sulfate (Pearson R=0.32, N=5940), which was also the case at the puy-de-Dome research station (1465 m a.s.l.) (Freney et al., 2011). The low Pearson correlation value can be partially explained by the extremely high concentration of OOA formed from the oxidation of organics emitted by biomass burning activities during the first week of the campaign. For the rest of campaign, the correlation value for sulfate with respect to OOA factor increased to 0.79 (N=3878), which is consistent with previous studies.

As shown in Fig. 6(a), the two OOA factors (OOA-BB and OOA) were very abundant, with a predominantly contribution of 87 % to the total OA mass. This is consistent with the high oxygen level in the total OA. During 80 % of the observation period, OA concentrations were lower than 5 μg m^{-3}, with strong contributions from secondary organic aerosols (OOA and OOA-BB) (Fig. 6 (b)). This indicates that the background site was predominated by organic aerosols formed through regional transportation.

4 Discussion

4.1 Identification of biomass burning events

Enhanced BC concentrations were used to help identifying periods influenced by biomass burning plumes (Bougiatioti et al., 2014). The BC concentration of 85 ng m^{-3} was taken as the background concentration at this site. It is the average concentration observed in the beginning of April (1st April to 4th April), when the strong wind scavenged pollutants of the whole region. Back trajectory and fire maps illustrate that the dominant air masses for this period was from north India with minor biomass burning activities (see Fig. 7(d)). This concentration is consistent with the two-year averaged background level measured at Southern Himalayas (Marinoni et al., 2010), and comparable to the lowest BC concentrations found over the southeastern Tibetan Plateau in the pre-monsoon season (Engling et al., 2011).

During the sampling period, three episodes were identified as being influenced by biomass burning, with the following criteria satisfied, i.e. (a) Back trajectory analysis shows a uniform source region; (b) Fire map shows fire spots in the region during the episode; (c) BC concentrations were higher than the background level of 85 ng m^{-3} determined above. One long-lasting and strong episode was from 22nd March to 30th March. The air masses arrived at the site during this period were from the north part of Myanmar, and covered active biomass burning areas (see Fig. 7(a)). As shown on the fire map, the site may also be influenced by wildfires in the vicinity. Two less intense events were observed on 5th – 6th April and 11th – 12th April, with slightly elevated BC concentrations. During the third event (11th – 12th April), the site experienced heavy snow. The back trajectory shows that air masses to this region were transported from regions with few fire spots. The enhanced BC concentration was probably emitted by biomass burning activities nearby for domestic heating and cooking.

These three biomass burning events were further validated by the increase of the fraction of biomass burning tracers, f_{60}. During the first and second events, the average f_{60} were 0.98 % and 0.61 %, respectively. These values were much lower than the f_{60} of 1.4 % during the third event, which was influenced by fires in the vicinity. This showed the decay of f_{60} in ambient plumes transported from sources to the receptor site. During the clean episode, the f_{60} decreased to about 0.4 %, indicating minor biomass burning influence (Cubison et al., 2011).

The box plot (Fig. 8) shows the concentrations of different chemical components of biomass burning events and background conditions. The aerosol concentrations corresponding to the background condition is highlighted by light gray. Organic aerosols are represented by the left axis while other species are represented by the right axis. Aerosols corresponding to biomass burning events were at high concentrations. The concentrations of organic aerosol during three biomass burning events were 10, 4 and 6-fold higher than that of the background condition. During the first event, due to co-occurrence of biomass burning activities in the vicinity together with the long-range transport of biomass burning plume, the concentration of BC reached 14 times higher than that of the background condition. All species remained low and sustained background concentrations during the clean episode, with an average PM_1 concentration of 1.2 $\mu g\ m^{-3}$.

4.2 Characteristic of three Biomass burning events

The comparison of OA fractions of different biomass burning events is shown in Fig. 9. Since the air masses arriving at Mt. Yulong during the second event were transported from active biomass burning areas in Myanmar within 48h, most of the freshly emitted BBOA were processed and transformed to more oxidized OA, with OOA and OOA-BB together accounting for 90 % on average of the total organic mass. Although the ratio of BBOA to the total OA during this event has a similar level to the background level, the mass concentrations of both OA and BBOA were more elevated than the background level. In contrast, the fraction of BBOA had strong enhancement during the third event, reaching 23 %. It is consistent with the previously mentioned identification that the biomass burning plumes were mainly from residential heating nearby, which could emit large amount of fresh BBOA.

The aging and/or mixing processes of different biomass burning plumes are further characterized in terms of the f_{44} vs. f_{60} triangle plot (Cubison et al., 2011). f_{44}, similarly defined to f_{60} as the ratio of the signal at m/z 44 to the total OA signal, is used here as an indicator of atmospheric aging, since OA and their gas phase precursors evolve in the atmosphere by becoming increasingly oxidized with higher CO_2^+ fraction (Jimenez et al., 2009;Ng et al., 2010). BBOA can be clearly distinguished from oxidized OA in the triangle plot. With the aging process of biomass burning plumes, OA evolved toward higher f_{44} and lower f_{60}, and gained more similar signature with OOA.

The OA clusters of three biomass burning events are shown clearly in the f_{44}-f_{60} triangle plot (Fig. 10). The OA clusters of the first and third events both present OA peaks with high f_{60} values, since the site was possibly influenced by residential heating in the surrounding regions during these two episodes. The OA cluster of the second event presents more similar oxidative properties to OOA and OOA-BB, due to loss of biomass burning marker through aging process during transport.

5 Conclusions

During the pre-monsoon season the aerosol evolution was explored at a high altitude receptor site on Mt. Yulong (3410 m a.s.l.) in the Tibetan Plateau in Southwestern China. The average concentration of PM_1 was 5.7 μg m^{-3}, which was far below that measured in urban and suburban as well as regional sites of China. The carbonaceous species (OA+BC) were very abundant in PM_1, with an average contribution of 77 %, followed by sulfate (14 %) and ammonium (5 %). This high altitude mountain site is suitable for tracing the influence of pollution plumes transported from the large areas of South Asia.

Using PMF analysis, organic aerosol was resolved into three factors, BBOA, OOA-BB and OOA. OOA-BB formed after atmospheric process of BBOA during long-range transport. The two oxygenated OA factors (OOA and OOA-BB) accounted for 87 % of the total OA, showing the highly oxidized nature of aerosol at the Mt. Yulong.

Different types of biomass burning events were identified by examining organic tracer in mass profiles and BC concentrations. The origins of biomass burning plumes were verified by analyzing the back trajectories of air masses as well as fire maps. Elevated PM_1 concentrations due to the transport of air pollutants from active biomass burning areas in South Asia were observed. Domestic heating activity also had interference on the background condition of Mt. Yulong.

This study provides clear evidence on the influence of the transport of pollutants emitted by biomass burning activity in South Asia on the southeastern edge of the Tibetan Plateau in China. The chemical characteristics of aerosols observed by in situ measurement can serve as inputs for model validations of aerosol-cloud processes and long-range transports. This study also highlights the impact of anthropogenic emissions to the pristine region of the Tibetan Plateau, which may influence global climate.

6 Data availability

The data presented in this article are available from the authors upon request (minhu@pku.edu.cn).

Acknowledgements

This study was supported by the National Natural Science Foundation of China (91544214, 21190052 and 41121004) and the China Ministry of Environmental Protection’s Special Funds for Scientific Research on Public Welfare (20130916). We also thank China National Environmental Monitoring Center for the support to the field campaign.

References

Aiken, A. C., DeCarlo, P. F., and Jimene, J. L.: Elemental Analysis of Organic Species with Electron Ionization High-Resolution Mass Spectrometry, Anal. Chem., 79, 8350-8358, 10.1021/ac071150w, 2007.

Aiken, A. C., Decarlo, P. F., Kroll, J. H., Worsnop, D. R., Huffman, J. A., Docherty, K. S., Ulbrich, I. M., Mohr, C., Kimmel, J. R., Sueper, D., Sun, Y., Zhang, Q., Trimborn, A., Northway, M., Ziemann, P. J., Canagaratna, M. R., Onasch, T. B., Alfarra,

M. R., Prevot, A. S. H., Dommen, J., Duplissy, J., Metzger, A., Baltensperger, U., and Jimenez, J. L.: O/C and OM/OC Ratios of Primary, Secondary, and Ambient Organic Aerosols with High-Resolution Time-of-Flight Aerosol Mass Spectrometry, Environ. Sci. Technol., 42, 10.1021/es703009q, 2008.

Bonasoni, P., Laj, P., Marinoni, A., Sprenger, M., Angelini, F., Arduini, J., Bonafè, U., Calzolari, F., Colombo, T., Decesari, S., Di Biagio, C., di Sarra, A. G., Evangelisti, F., Duchi, R., Facchini, M. C., Fuzzi, S., Gobbi, G. P., Maione, M., Panday, A., Roccato, F., Sellegri, K., Venzac, H., Verza, G. P., Villani, P., Vuillermoz, E., and Cristofanelli, P.: Atmospheric Brown Clouds in the Himalayas: first two years of continuous observations at the Nepal Climate Observatory-Pyramid (5079 m), Atmos. Chem. Phys., 10, 7515-7531, 10.5194/acp-10-7515-2010, 2010.

Bougiatioti, A., Stavroulas, I., Kostenidou, E., Zarmpas, P., Theodosi, C., Kouvarakis, G., Canonaco, F., Prévôt, A. S. H., Nenes, A., Pandis, S. N., and Mihalopoulos, N.: Processing of biomass-burning aerosol in the eastern Mediterranean during summertime, Atmos. Chem. Phys., 14, 4793-4807, 10.5194/acp-14-4793-2014, 2014.

Brito, J., Rizzo, L. V., Morgan, W. T., Coe, H., Johnson, B., Haywood, J., Longo, K., Freitas, S., Andreae, M. O., and Artaxo, P.: Ground-based aerosol characterization during the South American Biomass Burning Analysis (SAMBBA) field experiment, Atmos. Chem. Phys., 14, 12069-12083, 10.5194/acp-14-12069-2014, 2014.

Canagaratna, M. R., Jayne, J. T., Jimenez, J. L., Allan, J. D., Alfarra, M. R., Zhang, Q., Onasch, T. B., Drewnick, F., Coe, H., Middlebrook, A., Delia, A., Williams, L. R., Trimborn, A. M., Northway, M. J., DeCarlo, P. F., Kolb, C. E., Davidovits, P., and Worsnop, D. R.: Chemical and microphysical characterization of ambient aerosols with the aerodyne aerosol mass spectrometer, Mass Spectrom. Rev., 26, 185-222, 10.1002/mas.20115, 2007.

Canagaratna, M. R., Jimenez, J. L., Kroll, J. H., Chen, Q., Kessler, S. H., Massoli, P., Ruiz, L. H., Fortner, E., R.Williams, L., R.Wilson, K., Surratt, J. D., Donahue, N. M., Jayne, J. T., and R.Worsnop, D.: Elemental ratio measurements of organic compounds using aerosol mass spectrometry: characterization, improved calibration, and implications, Atmospheric Chemistry and Physics, 15, 253–272, 10.5194/acp-15-253-2015, 2015.

Cong, Z., Kang, S., Kawamura, K., Liu, B., Wan, X., Wang, Z., Gao, S., and Fu, P.: Carbonaceous aerosols on the south edge of the Tibetan Plateau: concentrations, seasonality and sources, Atmos. Chem. Phys., 15, 1573-1584, 10.5194/acp-15-1573-2015, 2015a.

Cong, Z., Kawamura, K., Kang, S., and Fu, P.: Penetration of biomass-burning emissions from South Asia through the Himalayas: new insights from atmospheric organic acids, Sci. Rep., 5, 9580, 10.1038/srep09580, 2015b.

Crippa, M., DeCarlo, P. F., Slowik, J. G., Mohr, C., Heringa, M. F., Chirico, R., Poulain, L., Freutel, F., Sciare, J., Cozic, J., Di Marco, C. F., Elsasser, M., Nicolas, J. B., Marchand, N., Abidi, E., Wiedensohler, A., Drewnick, F., Schneider, J., Borrmann, S., Nemitz, E., Zimmermann, R., Jaffrezo, J. L., Prevot, A. S. H., and Baltensperger, U.: Wintertime aerosol chemical composition and source apportionment of the organic fraction in the metropolitan area of Paris, Atmospheric Chemistry and Physics, 13, 961-981, 10.5194/acp-13-961-2013, 2013.

Cubison, M. J., Ortega, A. M., Hayes, P. L., Farmer, D. K., Day, D., Lechner, M. J., Brune, W. H., Apel, E., Diskin, G. S., Fisher, J. A., Fuelberg, H. E., Hecobian, A., Knapp, D. J., Mikoviny, T., Riemer, D., Sachse, G. W., Sessions, W., Weber, R. J., Weinheimer, A. J., Wisthaler, A., and Jimenez, J. L.: Effects of aging on organic aerosol from open biomass burning smoke in aircraft and laboratory studies, Atmospheric Chemistry and Physics, 11, 12049-12064, 10.5194/acp-11-12049-2011, 2011.

Decesari, S., Facchini, M. C., Carbone, C., Giulianelli, L., Rinaldi, M., Finessi, E., Fuzzi, S., Marinoni, A., Cristofanelli, P., Duchi, R., Bonasoni, P., Vuillermoz, E., Cozic, J., Jaffrezo, J. L., and Laj, P.: Chemical composition of PM_{10} and PM_1 at the high-altitude Himalayan station Nepal Climate Observatory-Pyramid (NCO-P) (5079 m a.s.l.), Atmos. Chem. Phys., 10, 4583-4596, 10.5194/acp-10-4583-2010, 2010.

Du, W., Sun, Y. L., Xu, Y. S., Jiang, Q., Wang, Q. Q., Yang, W., Wang, F., Bai, Z. P., Zhao, X. D., and Yang, Y. C.: Chemical characterization of submicron aerosol and particle growth events at a national background site (3295 m a.s.l.) on the Tibetan Plateau, Atmospheric Chemistry and Physics, 15, 10811-10824, 10.5194/acp-15-10811-2015, 2015.

Engling, G., and Gelencser, A.: Atmospheric Brown Clouds: From Local Air Pollution to Climate Change, Elements, 6, 223-228, 10.2113/gselements.6.4.223, 2010.

Engling, G., Zhang, Y.-N., Chan, C.-Y., Sang, X.-F., Lin, M., Ho, K.-F., Li, Y.-S., Lin, C.-Y., and Lee, J. J.: Characterization and sources of aerosol particles over the southeastern Tibetan Plateau during the Southeast Asia biomass-burning season, Tellus B, 63, 117-128, 10.1111/j.1600-0889.2010.00512.x, 2011.

Fröhlich, R., Cubison, M. J., Slowik, J. G., Bukowiecki, N., Canonaco, F., Croteau, P. L., Gysel, M., Henne, S., Herrmann, E., Jayne, J. T., Steinbacher, M., Worsnop, D. R., Baltensperger, U., and Prévôt, A. S. H.: Fourteen months of on-line measurements of the non-refractory submicron aerosol at the Jungfraujoch (3580 m a.s.l.) – chemical composition, origins and organic aerosol sources, Atmospheric Chemistry and Physics, 15, 11373-11398, 10.5194/acp-15-11373-2015, 2015.

Freney, E. J., Sellegri, K., Canonaco, F., Boulon, J., Hervo, M., Weigel, R., Pichon, J. M., Colomb, A., Prévôt, A. S. H., and Laj, P.: Seasonal variations in aerosol particle composition at the puy-de-Dôme research station in France, Atmos. Chem. Phys., 11, 13047-13059, 10.5194/acp-11-13047-2011, 2011.

He, L. Y., Lin, Y., Huang, X. F., Guo, S., Xue, L., Su, Q., Hu, M., Luan, S. J., and Zhang, Y. H.: Characterization of high-resolution aerosol mass spectra of primary organic aerosol emissions from Chinese cooking and biomass burning, Atmospheric Chemistry and Physics, 10, 11535-11543, 10.5194/acp-10-11535-2010, 2010.

Hu, W. W., Hu, M., Yuan, B., Jimenez, J. L., Tang, Q., Peng, J. F., Hu, W., Shao, M., Wang, M., Zeng, L. M., Wu, Y. S., Gong, Z. H., Huang, X. F., and He, L. Y.: Insights on organic aerosol aging and the influence of coal combustion at a regional receptor site of central eastern China, Atmospheric Chemistry and Physics, 13, 10095-10112, 10.5194/acp-13-10095-2013, 2013.

Hu, W. W., Hu, M., Hu, W., Jimenez, J. L., Yuan, B., Chen, W. T., Wang, M., Wu, Y. S., Chen, C., Wang, Z. B., Peng, J. F., Zeng, L. M., and Shao, M.: Chemical composition, sources, and aging process of submicron aerosols in Beijing: Contrast between summer and winter, JGRD, 121, 1955-1977, 10.1002/2015jd024020, 2016.

Huang, X.-F., Xue, L., Tian, X.-D., Shao, W.-W., Sun, T.-L., Gong, Z.-H., Ju, W.-W., Jiang, B., Hu, M., and He, L.-Y.: Highly time-resolved carbonaceous aerosol characterization in Yangtze River Delta of China: Composition, mixing state and secondary formation, Atmos. Environ., 64, 200-207, 10.1016/j.atmosenv.2012.09.059, 2013.

Huang, X. F., He, L. Y., Hu, M., Canagaratna, M. R., Sun, Y., Zhang, Q., Zhu, T., Xue, L., Zeng, L. W., Liu, X. G., Zhang, Y. H., Jayne, J. T., Ng, N. L., and Worsnop, D. R.: Highly time-resolved chemical characterization of atmospheric submicron particles during 2008 Beijing Olympic Games using an Aerodyne High-Resolution Aerosol Mass Spectrometer, Atmospheric

Chemistry and Physics, 10, 8933-8945, 10.5194/acp-10-8933-2010, 2010.

Huang, X. F., He, L. Y., Hu, M., Canagaratna, M. R., Kroll, J. H., Ng, N. L., Zhang, Y. H., Lin, Y., Xue, L., Sun, T. L., Liu, X. G., Shao, M., Jayne, J. T., and Worsnop, D. R.: Characterization of submicron aerosols at a rural site in Pearl River Delta of China using an Aerodyne High-Resolution Aerosol Mass Spectrometer, Atmospheric Chemistry and Physics, 11, 1865-1877, 10.5194/acp-11-1865-2011, 2011.

Huang, X. F., He, L. Y., Xue, L., Sun, T. L., Zeng, L. W., Gong, Z. H., Hu, M., and Zhu, T.: Highly time-resolved chemical characterization of atmospheric fine particles during 2010 Shanghai World Expo, Atmospheric Chemistry and Physics, 12, 4897-4907, 10.5194/acp-12-4897-2012, 2012.

IPCC: Climate change: the physical science basis, Cambridge University Press, Cambridge, England, 2013.

Jimenez, J. L., Canagaratna, M. R., Donahue, N. M., Prevot, A. S. H., Zhang, Q., Kroll, J. H., DeCarlo, P. F., Allan, J. D., Coe, H., Ng, N. L., Aiken, A. C., Docherty, K. S., Ulbrich, I. M., Grieshop, A. P., Robinson, A. L., Duplissy, J., Smith, J. D., Wilson, K. R., Lanz, V. A., Hueglin, C., Sun, Y. L., Tian, J., Laaksonen, A., Raatikainen, T., Rautiainen, J., Vaattovaara, P., Ehn, M., Kulmala, M., Tomlinson, J. M., Collins, D. R., Cubison, M. J., Dunlea, J., Huffman, J. A., Onasch, T. B., Alfarra, M. R., Williams, P. I., Bower, K., Kondo, Y., Schneider, J., Drewnick, F., Borrmann, S., Weimer, S., Demerjian, K., Salcedo, D., Cottrell, L., Griffin, R., Takami, A., Miyoshi, T., Hatakeyama, S., Shimono, A., Sun, J. Y., Zhang, Y. M., Dzepina, K., Kimmel, J. R., Sueper, D., Jayne, J. T., Herndon, S. C., Trimborn, A. M., Williams, L. R., Wood, E. C., Middlebrook, A. M., Kolb, C. E., Baltensperger, U., and Worsnop, D. R.: Evolution of Organic Aerosols in the Atmosphere, Science, 326, 1525-1529, 10.1126/science.1180353, 2009.

Jolleys, M. D., Coe, H., McFiggans, G., Taylor, J. W., O’Shea, S. J., Breton, M. L., Bauguitte, S. J.-B., Moller, S., Carlo, P. D., Aruffo, E., Palmer, P. I., Lee, J. D., Percival, C. J., and Gallagher, M. W.: Properties and evolution of biomass burning organic aerosol from Canadian boreal forest fire, Atmos. Chem. Phys., 15, 3077-3095, 10.5194/acp-15-3077-2015, 2015.

Lüthi, Z. L., Škerlak, B., Kim, S. W., Lauer, A., Mues, A., Rupakheti, M., and Kang, S.: Atmospheric brown clouds reach the Tibetan Plateau by crossing the Himalayas, Atmos. Chem. Phys., 15, 6007-6021, 10.5194/acp-15-6007-2015, 2015.

Lau, W. K. M., Kim, M.-K., Kim, K.-M., and Lee, W.-S.: Enhanced surface warming and accelerated snow melt in the Himalayas and Tibetan Plateau induced by absorbing aerosols, Environ. Res. Lett., 5, 025204, 10.1088/1748-9326/5/2/025204, 2010.

Li, Y. J., Lee, B. P., Su, L., Fung, J. C. H., and Chan, C. K.: Seasonal characteristics of fine particulate matter (PM) based on high-resolution time-of-flight aerosol mass spectrometric HR-ToF-AMS) measurements at the HKUST Supersite in Hong Kong, Atmospheric Chemistry and Physics, 15, 37–53, 10.5194/acp-15-37-2015, 2015.

Marinoni, A., Cristofanelli, P., Laj, P., Duchi, R., Calzolari, F., Decesari, S., Sellegri, K., Vuillermoz, E., Verza, G. P., Villani, P., and Bonasoni, P.: Aerosol mass and black carbon concentrations, a two year record at NCO-P (5079 m, Southern Himalayas), Atmos. Chem. Phys., 10, 8551-8562, 10.5194/acp-10-8551-2010, 2010.

Middlebrook, A. M., Bahreini, R., Jimenez, J. L., and Canagaratna, M. R.: Evaluation of Composition-Dependent Collection Efficiencies for the Aerodyne Aerosol Mass Spectrometer using Field Data, Aerosol Sci. Technol., 46, 258-271, 10.1080/02786826.2011.620041, 2012.

Ming, J., Xiao, C., Sun, J., Kang, S., and Bonasoni, P.: Carbonaceous particles in the atmosphere and precipitation of the Nam Co region, central Tibet, J. Environ. Sci., 22, 1748-1756, 10.1016/s1001-0742(09)60315-6, 2010.

Minguillón, M. C., Ripoll, A., Pérez, N., Prévôt, A. S. H., Canonaco, F., Querol, X., and Alastuey, A.: Chemical characterization of submicron regional background aerosols in the western Mediterranean using an Aerosol Chemical Speciation Monitor, Atmospheric Chemistry and Physics, 15, 6379-6391, 10.5194/acp-15-6379-2015, 2015.

Ng, N. L., Canagaratna, M. R., Zhang, Q., Jimenez, J. L., Tian, J., Ulbrich, I. M., Kroll, J. H., Docherty, K. S., Chhabra, P. S., Bahreini, R., Murphy, S. M., Seinfeld, J. H., Hildebrandt, L., Donahue, N. M., DeCarlo, P. F., Lanz, V. A., Prévôt, A. S. H., Dinar, E., Rudich, Y., and Worsnop, D. R.: Organic aerosol components observed in Northern Hemispheric datasets from Aerosol Mass Spectrometry, Atmospheric Chemistry and Physics, 10, 4625-4641, 10.5194/acp-10-4625-2010, 2010.

Paatero, P., and Tapper, U.: Positive matrix factorization: A non-negative factor model with optimal utilization of error estimates of data values, Environmetrics, 5, 111-126, 10.1002/env.3170050203, 1994.

Qian, Y., Flanner, M. G., Leung, L. R., and Wang, W.: Sensitivity studies on the impacts of Tibetan Plateau snowpack pollution on the Asian hydrological cycle and monsoon climate, Atmos. Chem. Phys., 11, 1929-1948, 10.5194/acp-11-1929-2011, 2011.

Ripoll, A., Minguillón, M. C., Pey, J., Jimenez, J. L., Day, D. A., Sosedova, Y., Canonaco, F., Prévôt, A. S. H., Querol, X., and Alastuey, A.: Long-term real-time chemical characterization of submicron aerosols at Montsec (southern Pyrenees, 1570ma.s.l.), Atmos. Chem. Phys., 15, 2935–2951, 10.5194/acp-15-2935-2015, 2015.

Sjogren, S., Gysel, M., E.Weingartner, Alfarra, M. R., Duplissy, J., Cozic, J., Crosier, J., Coe, H., and Baltensperger, U.: Hygroscopicity of the submicrometer aerosol at the high-alpine site Jungfraujoch, 3580m a.s.l., Switzerland, Atmos. Chem. Phys., 8, 5715–5729, 10.5194/acp-8-5715-2008, 2008.

Streets, D. G., Yarber, K. F., Woo, J. H., and Carmichael, G. R.: Biomass burning in Asia: Annual and seasonal estimates and atmospheric emissions, Global Biogeochem. Cycles, 17, 1759-1768, 10.1029/2003gb002040, 2003.

Sun, Y. L., Zhang, Q., Schwab, J. J., Demerjian, K. L., Chen, W. N., Bae, M. S., Hung, H. M., Hogrefe, O., Frank, B., Rattigan, O. V., and Lin, Y. C.: Characterization of the sources and processes of organic and inorganic aerosols in New York city with a high-resolution time-of-flight aerosol mass apectrometer, Atmospheric Chemistry and Physics, 11, 1581-1602, 10.5194/acp-11-1581-2011, 2011.

Ulbrich, I. M., Canagaratna, M. R., Zhang, Q., Worsnop, D. R., and Jimenez, J. L.: Interpretation of organic components from Positive Matrix Factorization of aerosol mass spectrometric data, Atmospheric Chemistry and Physics, 9, 2891-2918, 10.5194/acp-9-2891-2009, 2009.

von Schneidemesser, E., Monks, P. S., Allan, J. D., Bruhwiler, L., Forster, P., Fowler, D., Lauer, A., Morgan, W. T., Paasonen, P., Righi, M., Sindelarova, K., and Sutton, M. A.: Chemistry and the Linkages between Air Quality and Climate Change, Chem. Rev., 115, 3856-3897, 10.1021/acs.chemrev.5b00089, 2015.

Wan, X., Kang, S., Wang, Y., Xin, J., Liu, B., Guo, Y., Wen, T., Zhang, G., and Cong, Z.: Size distribution of carbonaceous aerosols at a high-altitude site on the central Tibetan Plateau (Nam Co Station, 4730ma.s.l.), Atmos. Res., 153, 155-164, 10.1016/j.atmosres.2014.08.008, 2015.

Wang, B., and French, H. M.: Climate Controls and High-Altitude Permafrost, Qinghai-Xizang (Tibet) Plateau, China, Permafrost and Periglacial Processes, 5, 87-100, 10.1002/ppp.3430050203, 1994.

Wang, B., Liu, Y., Shao, M., Lu, S., Wang, M., Yuan, B., Gong, Z., He, L., Zeng, L., Hu, M., and Zhang, Y.: The contributions of biomass burning to primary and secondary organics: A case study in Pearl River Delta (PRD), China, Sci. Total. Environ., 569-570, 548-556, 10.1016/j.scitotenv.2016.06.153, 2016.

Xia, X., Zong, X., Cong, Z., Chen, H., Kang, S., and Wang, P.: Baseline continental aerosol over the central Tibetan plateau and a case study of aerosol transport from South Asia, Atmos. Environ., 45, 7370-7378, 10.1016/j.atmosenv.2011.07.067, 2011.

Xu, J., Zhang, Q., Li, X., Ge, X., Xiao, C., Ren, J., and Qin, D.: Dissolved organic matter and inorganic ions in a central Himalayan glacier--insights into chemical composition and atmospheric sources, Environ. Sci. Technol., 47, 6181-6188, 10.1021/es4009882, 2013.

Xu, J., Wang, Z., Yu, G., Qin, X., Ren, J., and Qin, D.: Characteristics of water soluble ionic species in fine particles from a high altitude site on the northern boundary of Tibetan Plateau: Mixture of mineral dust and anthropogenic aerosol, Atmos. Res., 143, 43-56, 10.1016/j.atmosres.2014.01.018, 2014a.

Xu, J., Zhang, Q., Chen, M., Ge, X., Ren, J., and Qin, D.: Chemical composition, sources, and processes of urban aerosols during summertime in northwest China: insights from high-resolution aerosol mass spectrometry, Atmospheric Chemistry and Physics, 14, 12593-12611, 10.5194/acp-14-12593-2014, 2014b.

Xu, J. Z., Zhang, Q., Wang, Z. B., Yu, G. M., Ge, X. L., and Qin, X.: Chemical composition and size distribution of summertime $PM_{2.5}$ at a high altitude remote location in the northeast of the Qinghai–Xizang (Tibet) Plateau: insights into aerosol sources and processing in free troposphere, Atmospheric Chemistry and Physics, 15, 5069-5081, 10.5194/acp-15-5069-2015, 2015.

You, C., Xu, C., Xu, B., Zhao, H., and Song, L.: Levoglucosan evidence for biomass burning records over Tibetan glaciers, Environ. Pollu., 216, 173-181, 10.1016/j.envpol.2016.05.074, 2016.

Zhang, Q., Jimenez, J. L., Canagaratna, M. R., Ulbrich, I. M., Ng, N. L., Worsnop, D. R., and Sun, Y.: Understanding atmospheric organic aerosols via factor analysis of aerosol mass spectrometry: a review, Anal Bioanal Chem, 401, 3045-3067, 10.1007/s00216-011-5355-y, 2011.

Zhang, Y., Tang, L., Wang, Z., Yu, H. X., Sun, Y. L., Liu, D., Qin, W., Canonaco, F., Prévôt, A. S. H., Zhang, H. L., and Zhou, H. C.: Insights into characteristics, sources, and evolution of submicron aerosols during harvest seasons in the Yangtze River delta region, China, Atmospheric Chemistry and Physics, 15, 1331-1349, 10.5194/acp-15-1331-2015, 2015.

Zhao, Z., Cao, J., Shen, Z., Xu, B., Zhu, C., Chen, L. W. A., Su, X., Liu, S., Han, Y., Wang, G., and Ho, K.: Aerosol particles at a high-altitude site on the Southeast Tibetan Plateau, China: Implications for pollution transport from South Asia, J. Geophys. Res. Atmos, 118, 11,360-311,375, 10.1002/jgrd.50599, 2013.

Table 1. Comparison between mass spectra of different OA with reference spectra.

	Reference spectra	Pearson Correlation Coefficient (N=100)			Citation
		BBOA	OOA-BB	OOA	
Ambient measurement	900m above fire	0.91	0.56	0.34	Brito et al. (2014)
	3h downwind	0.51	0.97	0.91	Brito et al. (2014)
	MO-OOA	0.69	0.86	0.69	Hu et al. (2016)
	BBOA	0.85	0.38	0.11	Hu et al. (2016)
Laboratory simulation	wood of pin	0.91	0.61	0.42	He et al. (2010)
	rice straw	0.94	0.6	0.36	He et al. (2010)

Figure 1. The location of the sampling site at Mt. Yulong (27.2 °N 100.2 °E, 3410 m a.s.l.).

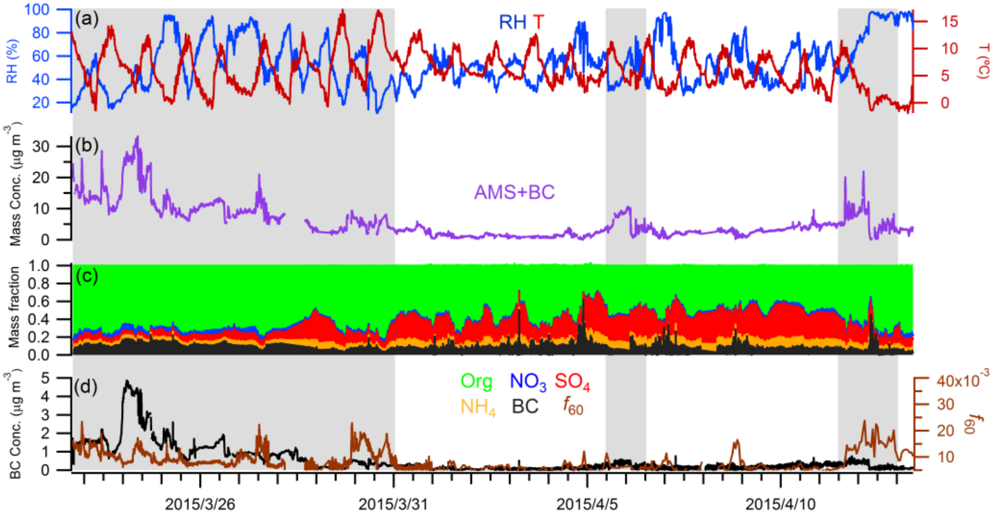

Figure 2. Time series of (a) relative humidity and temperature; (b) total mass concentrations from AMS plus black carbon (c) mass fractions of different chemical species; (d) concentrations of black carbon and f_{60}. The gray background denotes three biomass burning events (identified in Sect. 4.1).

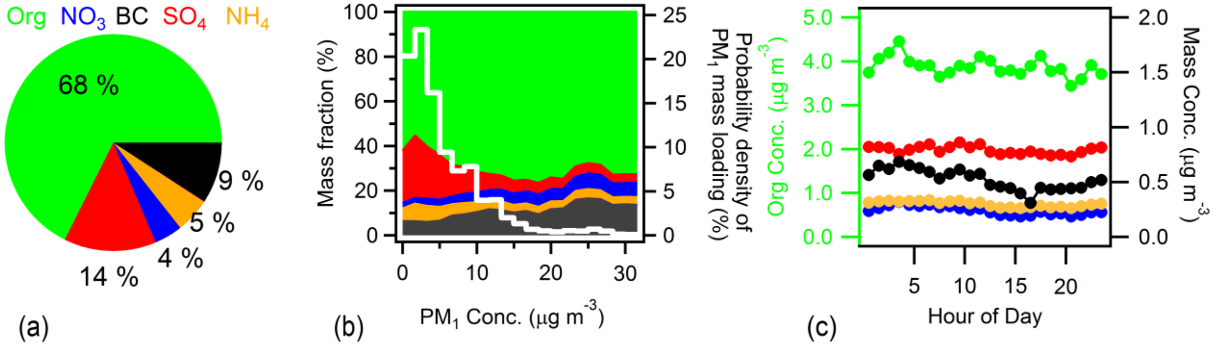

Figure 3. (a) average chemical composition of the whole campaign; (b) the mass fractions of PM_1 species as a function of PM_1 mass loading (left axis), with the white line representing the probability density of PM_1 mass loadings (right axis); (c) the diel cycle of different species, with the left axis for organics, and the right axis for the rest components.

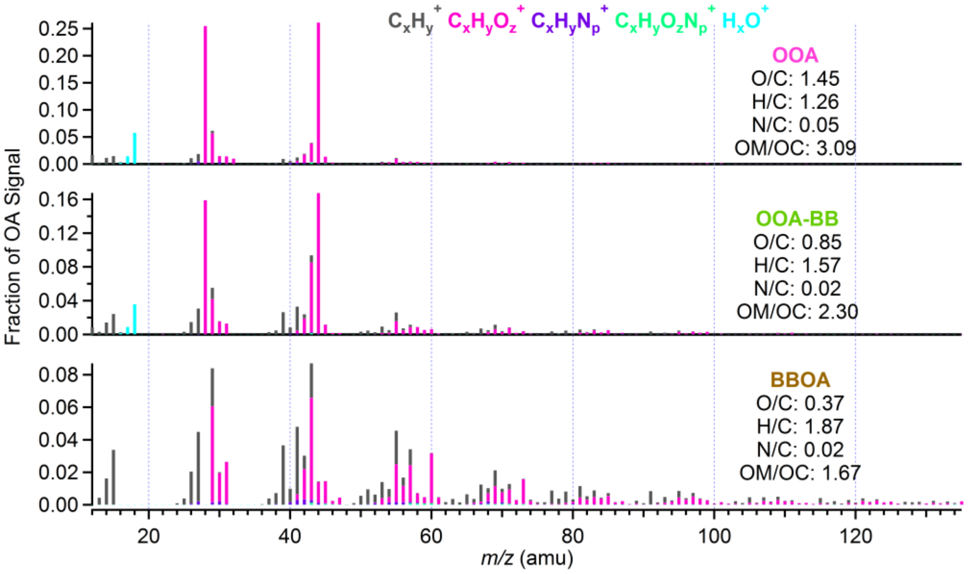

Figure 4. The mass spectra of each factor resolved by PMF, together with atomic ratios of each factor.

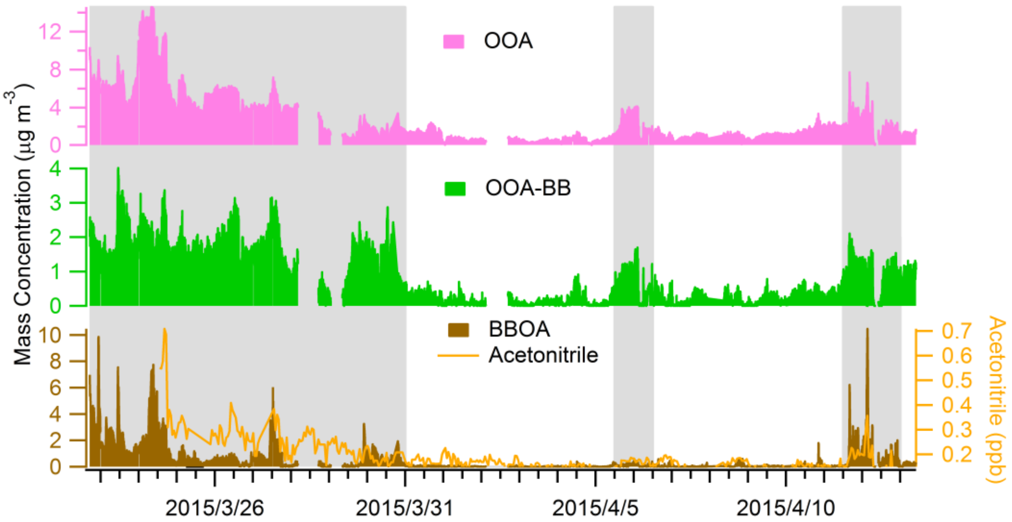

Figure 5. The time series of three OA factors resolved by PMF, together with acetonitrile. The grey background areas denote the biomass burning events (identified in Sect. 4.1).

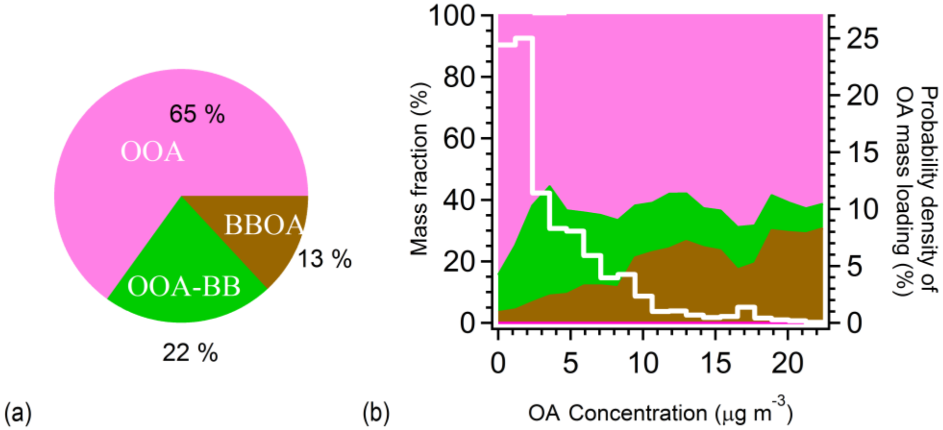

Figure 6. (a) contribution of each factor to the total OA mass; (b) fractions of OA factor (left axis) and probability density of OA concentration (white line, right axis) as a function of OA mass loading.

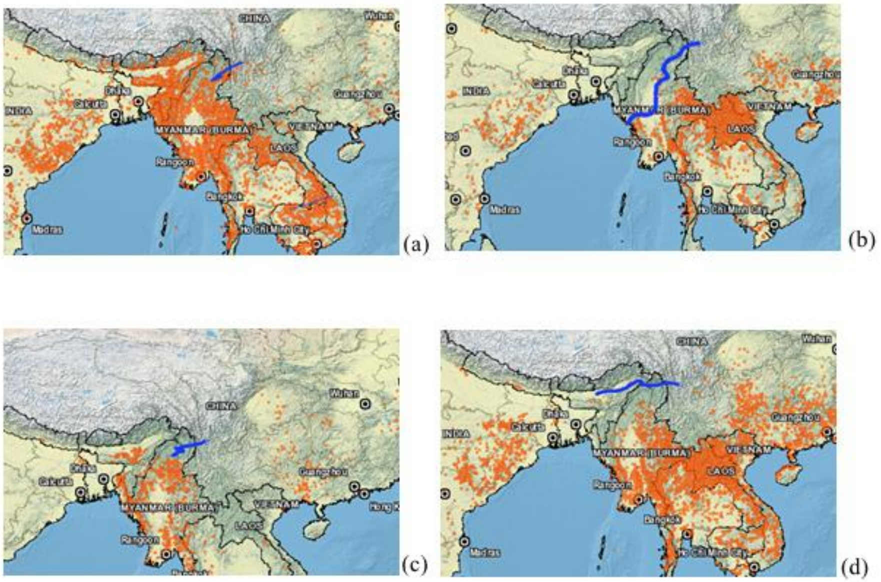

Figure 7. Occurrence of wildfire derived from MODIS images and back trajectories (blue lines) from WRF model (a) first biomass burning event: March 22nd–30th; (b) second biomass burning event: April 5th–6th; (c) third biomass burning event: April 11th–12th; (d) background: April 1st–4th.

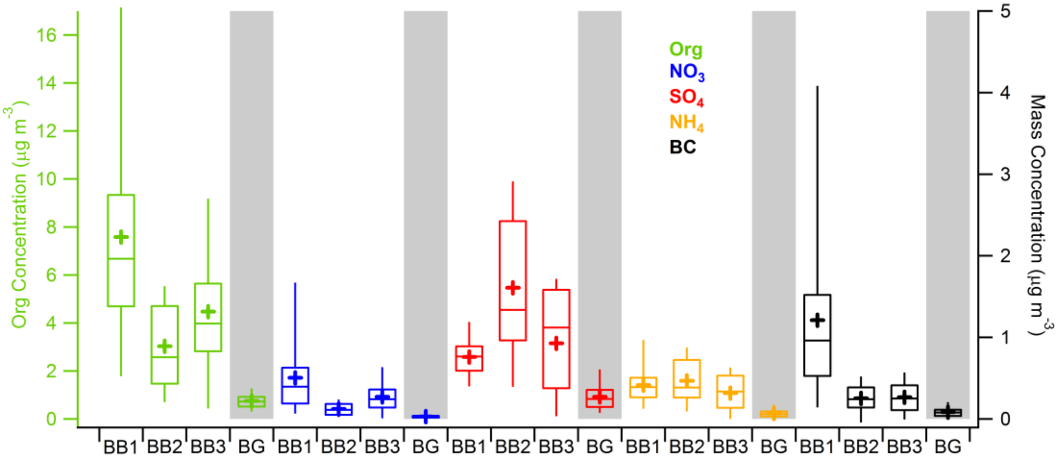

Figure 8. Comparison of chemical compositions between three biomass burning events (BB1, BB2, BB3) and background conditions (BG,

highlighted by light gray color). Boxes denote median, 25th and 75th percentiles; whiskers represent 5th and 95th percentiles; crosses represent mean values. Organic aerosols are represented by the left axis while other species are represented by the right axis.

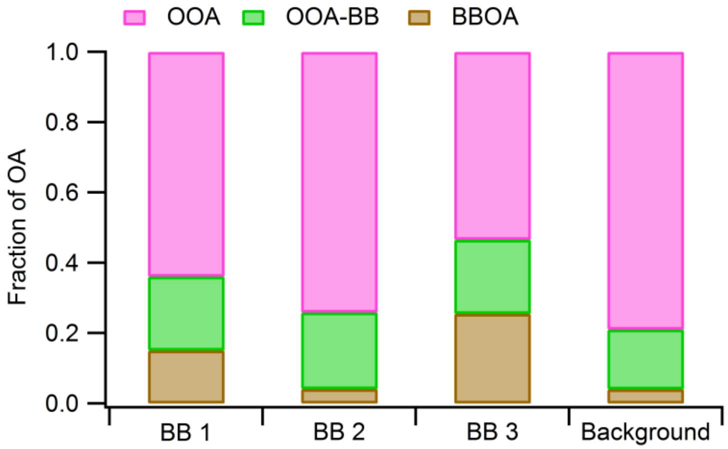

Figure 9. The relative contribution of different types of OA during three biomass burning events and background condition.

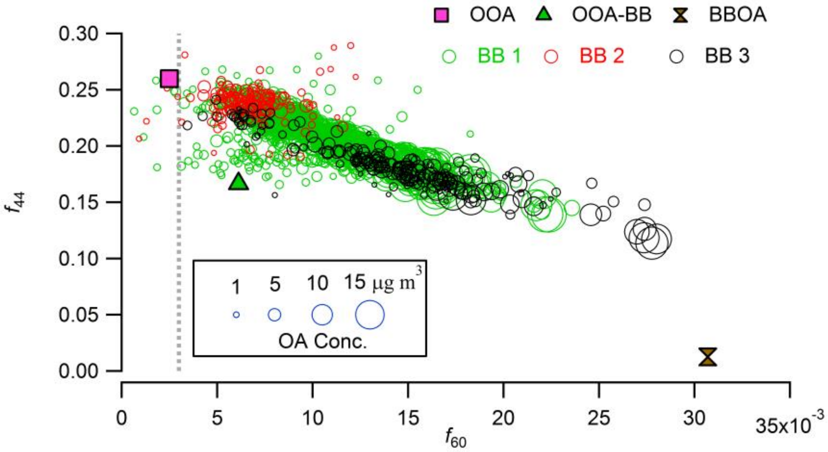

Figure 10. *f*44 as a function of *f* 60 (*f*44 vs. *f*60 triangle plot) of the three biomass burning events, sized by OA concentration.